Electronic Supplementary Information (ESI)

Oxidation-Induced Phase Transformations of Hybrid Tin Bromide Single Crystals Enable the Occurrence of Second-Harmonic Generation

Binyin Yu,[a] Can Yang,[b] Zhexin Song,[a] Guokui Liu, *[c] Jing Wei,[d] Qi Wu, *[b] and Yangyang Dang*[a]

[a]School of Physics and Physical Engineering, Shandong Provincial Key Laboratory of Laser Polarization and Information Technology, Qufu Normal University, Qufu, Shandong 273165, P. R. China. Email: dyy@qfnu.edu.cn

[b]Hubei Key Laboratory of Pollutant Analysis & Reuse Technology, College of Chemistry and Chemical Engineering, Hubei Normal University, Huangshi, Hubei 435002, China. Email: wuqi2011@whu.edu.cn

[c]School of Chemistry and Chemical Engineering, Linyi University, Linyi 276000, P. R. China. Email: liuguokuihappy@163.com

[d]Beijing Key Laboratory of Construction-Tailorable Advanced Functional Materials and Green Applications, Experimental Center of Advanced Materials School of Materials Science and Engineering, Beijing Institute of Technology, Beijing 100081, P. R. China

Corresponding Authors:
Email：dyy@qfnu.edu.cn (Y. D.); wuqi2011@whu.edu.cn (Q. W.); liuguokuihappy@163.com (G. L.)

Table of contents

Characterizations

Powder and Single Crystal X-ray Diffraction Measurements. Powder X-ray diffraction patterns were measured on a PANalytical XPert Pro MPD equipment with Cu-K_a radiation in the 2θ range of 10-80° using reasonable step size and step time settings. Single-crystal X-ray diffraction data were collected on a Bruker D8 advance diffractometer equipped with a CCD detector (graphite-monochromated Mo-K_a radiation, λ= 0.71073 Å) at 293(2) K. APEX3 software was used for data integration and cell refinements. The crystal was kept at 293(2) K during data collection. Using Olex2,[1] the structure was solved with the Olex2.solve[2] structure solution program using Charge Flipping and refined with the XL [3] refinement package using Least Squares minimization.

X-ray Photoelectron Spectroscopy (XPS) Measurements. Polycrystalline samples were extracted using a sample transporter that protects against air exposure. The sample transporter is connected to the ultra-high vacuum chamber and then transferred to the XPS systems for characterizations. Pass energy values are 160 eV for XPS wide scan, 10 eV for high resolution scan. All the data analysis about XPS was performed using the XPS Peaks Fit software. All the elements were fitted with the 80% Gaussian and 20% Lorentzian peak shapes after applying background subtractions with Shirley function.[4]

Thermogravimetric Analysis (TGA) and Differential Scan Calorimetry (DSC) Measurements. Thermogravimetric analysis (TGA) was carried out using a TGA/DSC1/1600HT analyzer (METTLER TOLEDO Instruments). The powder samples were placed in Al_2O_3 crucible, and heated at a rate of 10 °C min^{-1} from room temperature to 600 °C under flowing N_2 gas, respectively. Differential Scan calorimetry (DSC) measurements were performed on Polyma Instruments (DSC-200-F3 Maia).

IR and ^{1}H-NMR, ^{13}C-NMR, measurements of $DMESnBr_n$ (n=4 or 6) and $TMDPSn_nBr_6$ (n=1 or 2). IR measurement of $DMESnBr_n$ (n=4 or 6) and $TMDPSn_nBr_6$ (n=1 or 2) was performed using KBr pellet method. The ^{1}H and ^{13}C Nuclear Magnetic Resonance (NMR) spectra of $DMESnBr_n$ (n=4 or 6) and $TMDPSn_nBr_6$ (n=1 or 2) were recorded in D6-dimethyl sulfoxide (DMSO) using a Bruker Advance 300 spectrometer. The data was delt and analysed with Mestre Nova software.

UV-Vis Diffuse Reflectance Spectroscopy. The UV-vis diffuse reflectance spectra of these compounds were recorded at room temperature on a Shimadzu UV-2600 UV-vis spectrophotometer in the wavelength range of 200-800 nm. $BaSO_4$ powder was used as 100% reflectance reference. The Kubelka-Munk function 3, 4 was used to calculate the absorption spectra from the reflection spectra: $F(R) = \alpha/S = (1-R)^2/2R$, where R is the reflectance, α is the absorption coefficient, and S is the scattering coefficient.

Second-Harmonic Generation Measurements. The Kurtz and Perry method was used to measure powder second harmonic generation (SHG) signals at room temperature.[5] The SHG efficiency mainly depends on the particle size, and the crystalline compound was ground and divided into the following particle sizes: 20-60, 60-100, 100-125, 125-150, 150-200, 200-300, and 300-400 μm. Microcrystalline KH_2PO_4 (KDP) with the same particle size was used as a reference. The measurements were performed using Q-switched Nd: YAG lasers with visible light at 1064 nm, and a cut-off filter was used to limit the background flash light on the sample, and the SHG signal is recorded by a photomultiplier tube.

Piezoelectricity measurement. We thus used the PiezoTest to investigate its piezoelectric performance through the quasi-static method. The $DMESnBr_6$ crystal were placed between two

copper foil electrodes and encapsulated with the polyethylene terephthalate (PET) tape to form a simple sandwich-structure powder piezoelectric device, as shown in **Fig. 5**. When the tapping frequency is 110 Hz, the d_{22} value was measured to be ±3 pC/N along the [010] direction for the crystal $DMESnBr_6$.

Simulation details. Structural optimization was performed via the Vienna ab initio simulation package (VASP)[6, 7] with the conjugate gradient method. The Perdew, Burke, and Ernzerhof exchange-correlation functional within GGA was used.[8, 9] The convergence of energy between two electronic steps in the self-consistent process was set to 10^{-5} eV. Ionic relaxation was stopped when the maximum force was smaller than 0.01 eV/Å. All atoms in the models and cell shape and volume were fully relaxed. The Monkhorst-Pack grids of 2×2×6 ($DMESnBr_4$) and 5×2×4 ($DMESnBr_6$) were used for the reciprocal space sampling.[10] An energy cutoff of 450 eV was adopted for plane-wave expansion of electronic wave functions.

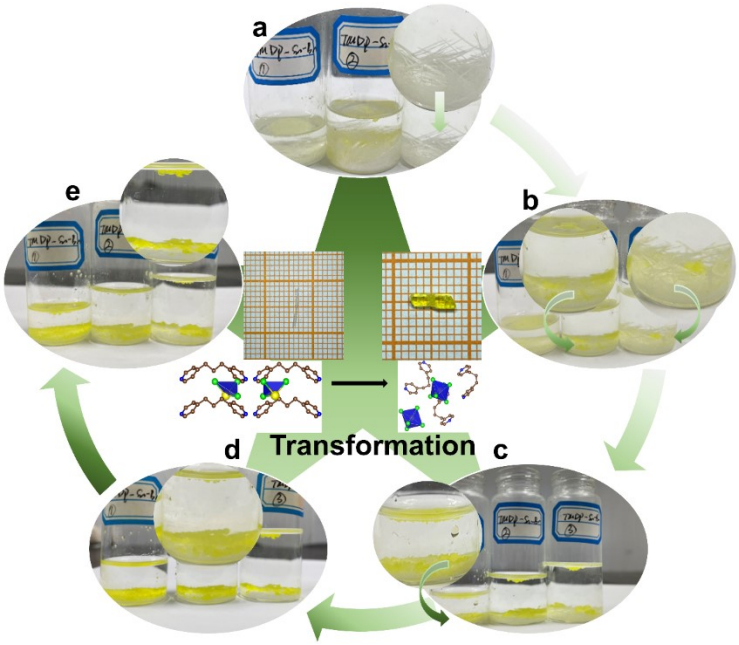

Fig. S1. Phase transformation process of $TMDPSn_2Br_6$ and $TMDPSnBr_6$ single crystals.

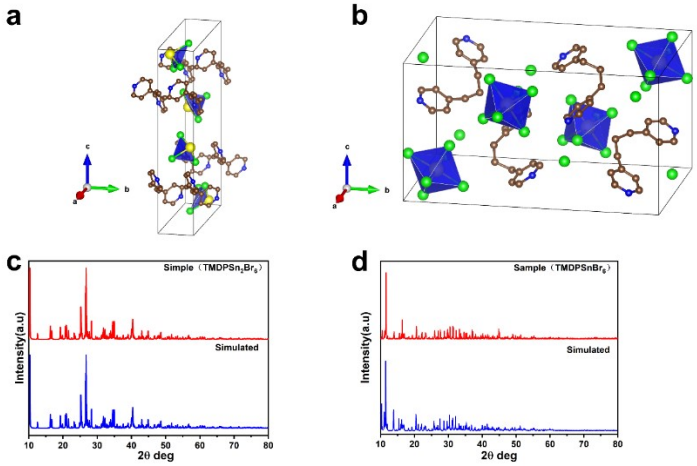

Fig. S2. Crystal structures and XRD patterns of $TMDPSn_2Br_6$ and $TMDPSnBr_6$. (a) ball−stick diagrams of $TMDPSn_2Br_6$, Note that H atoms bonded to the C or N atoms are omitted for clarity; b) ball−stick diagrams of $TMDPSnBr_6$; (c) powder and simulated XRD patterns of $TMDPSn_2Br_6$; (d) powder and simulated XRD patterns of $TMDPSnBr_6$.

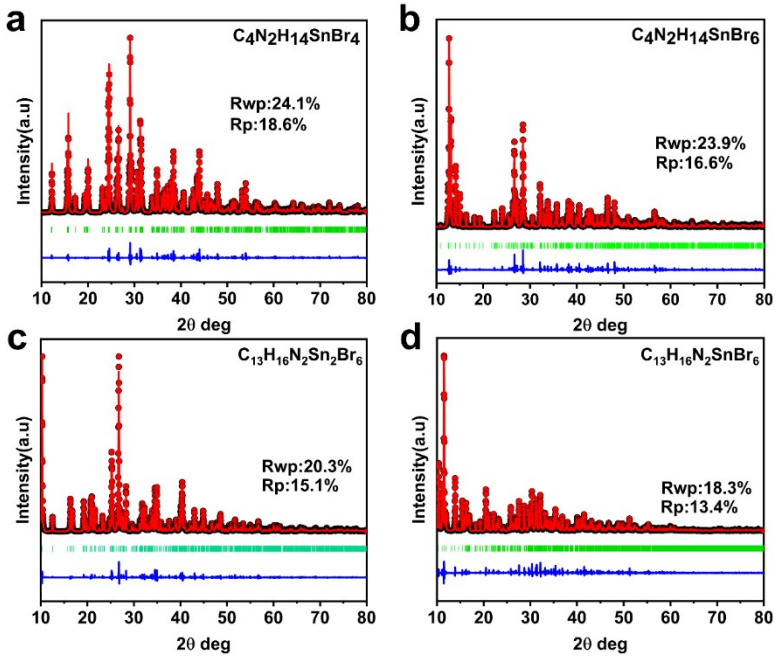

Fig. S3. Rietveld refined PXRD profile of (a) $DMESnBr_4$. (b) $DMESnBr_6$. (c) $TMDPSn_2Br_6$. (d) $TMDPSnBr_6$.

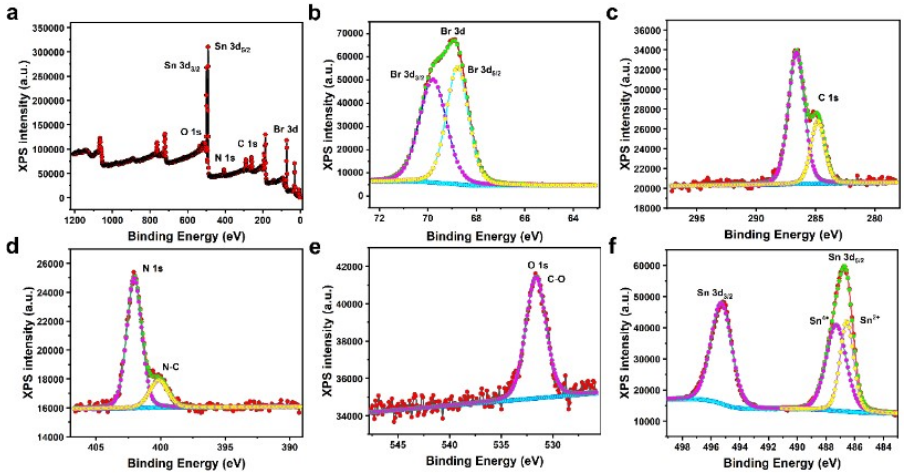

Fig. S4. Core level XPS spectra for $DMESnBr_4$. (a) wide scan, (b) Br 3d, (c) C 1s, (d) N 1s, (e) O 1s and (f) Sn 3d, fitted with peaks having an 80 % Gaussian and 20 % Lorentzian peak shape after applying background subtraction with *Shirley function*.

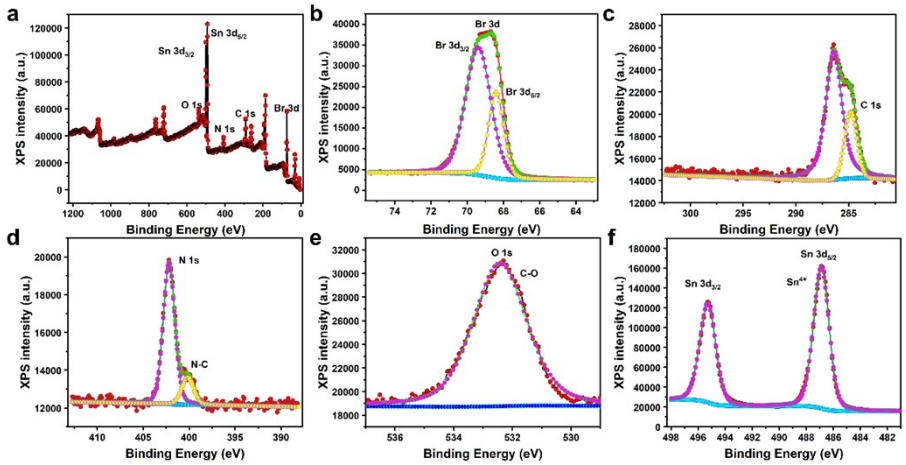

Fig. S5. Core level XPS spectra for $DMESnBr_6$. (a) wide scan, (b) Br 3d, (c) C 1s, (d) N 1s, (e) O 1s and (f) Sn 3d, fitted with peaks having an 80 % Gaussian and 20 % Lorentzian peak shape after applying background subtraction with *Shirley function*.

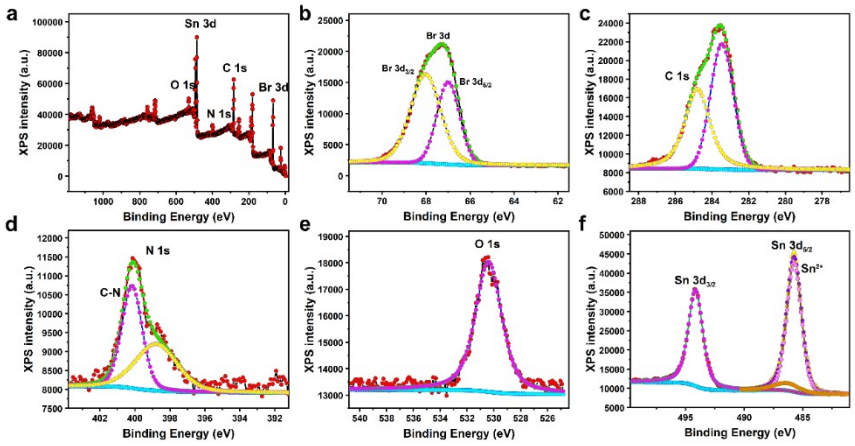

Fig. S6. Core level XPS spectra for $TMDPSn_2Br_6$. (a) wide scan, (b) Br 3d, (c) C 1s, (d) N 1s, (e) O 1s and (f) Sn 3d, fitted with peaks having an 80 % Gaussian and 20 % Lorentzian peak shape after applying background subtraction with *Shirley function.*

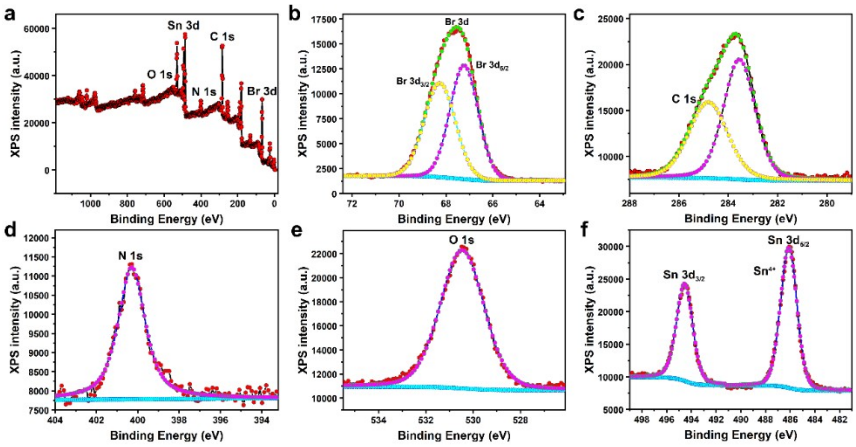

Fig. S7. Core level XPS spectra for $TMDPSnBr_6$. (a) wide scan, (b) Br 3d, (c) C 1s, (d) N 1s, (e) O 1s and (f) Sn 3d, fitted with peaks having an 80 % Gaussian and 20 % Lorentzian peak shape after applying background subtraction with *Shirley function*.

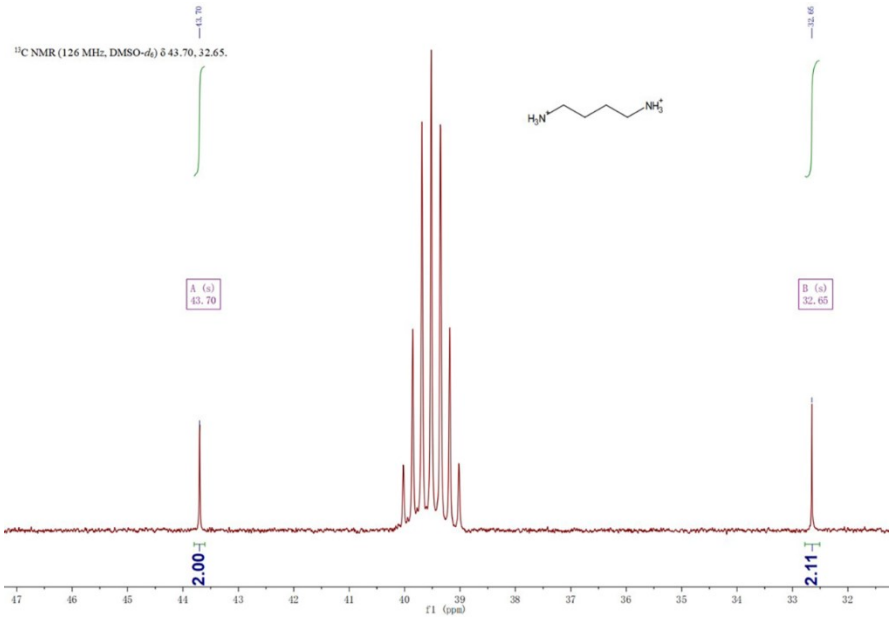

Fig. S8. ^{13}C-NMR of $DMESnBr_4$ measured in DMSO-d6.

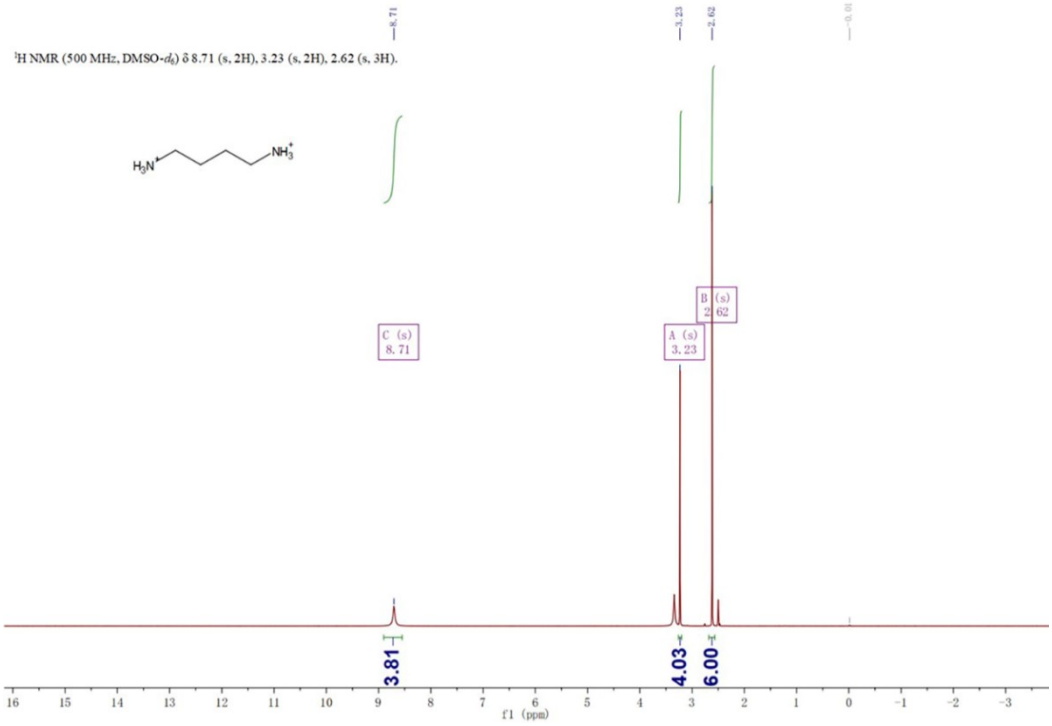

Fig. S9. ^{1}H-NMR of $DMESnBr_4$ measured in DMSO-d6.

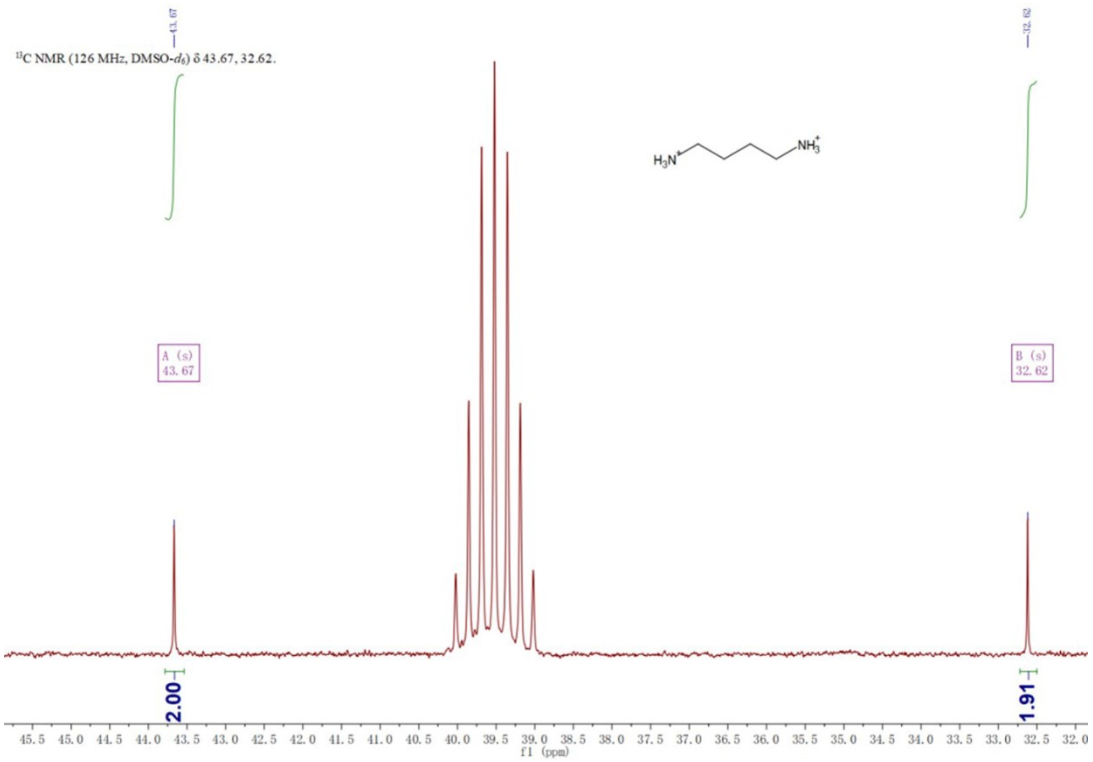

Fig. S10. ^{13}C-NMR of $DMESnBr_6$ measured in DMSO-d6.

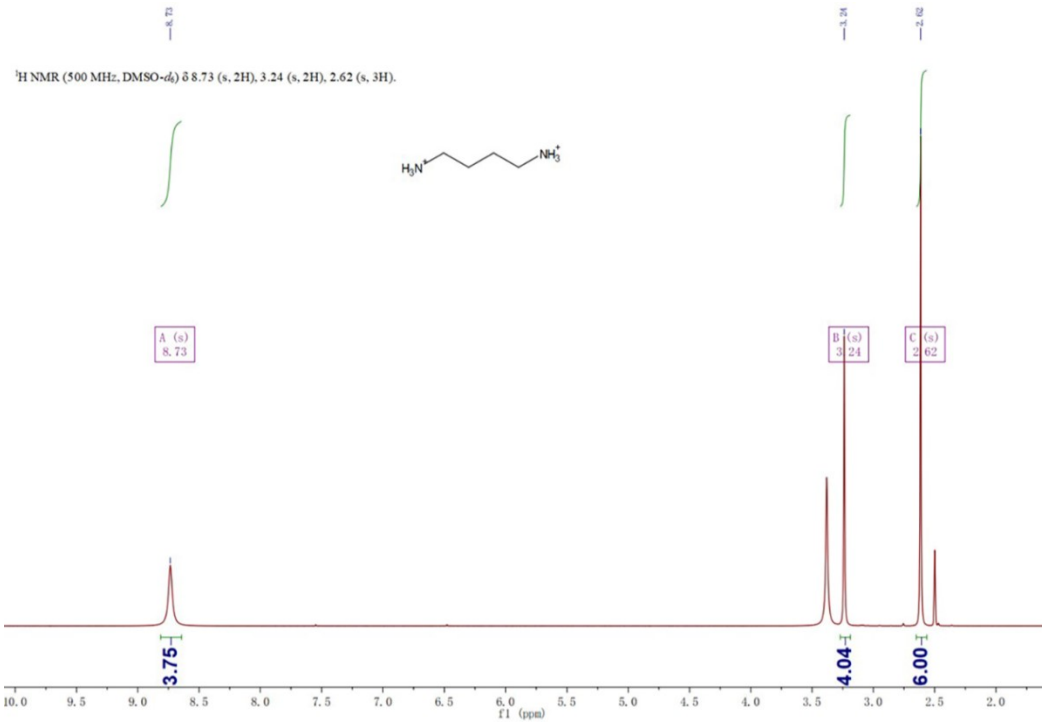

Fig. S11. ^{1}H-NMR of $DMESnBr_6$ measured in DMSO-d6.

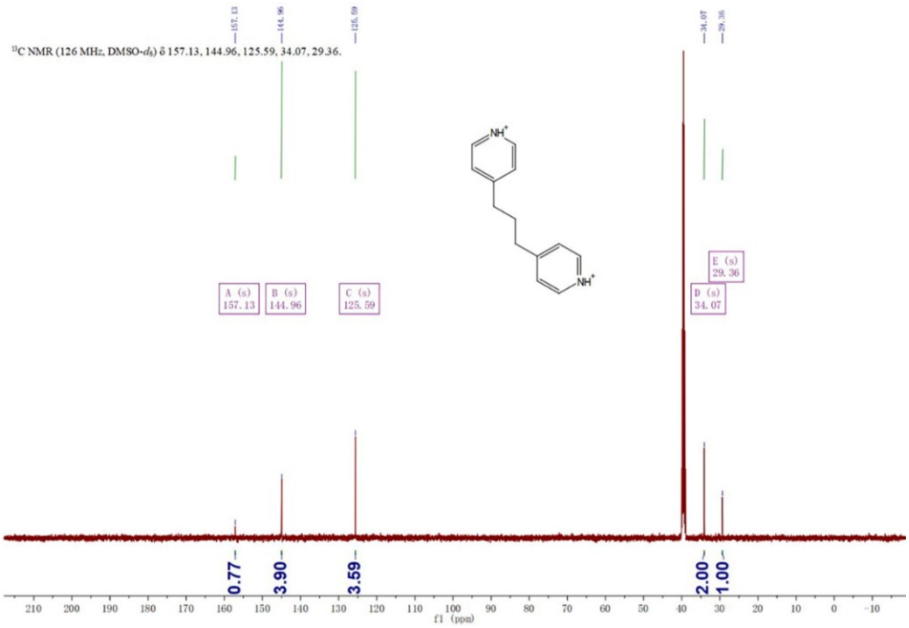

Fig. S12. ^{13}C-NMR of $TMDPSn_2Br_6$ measured in DMSO-d6.

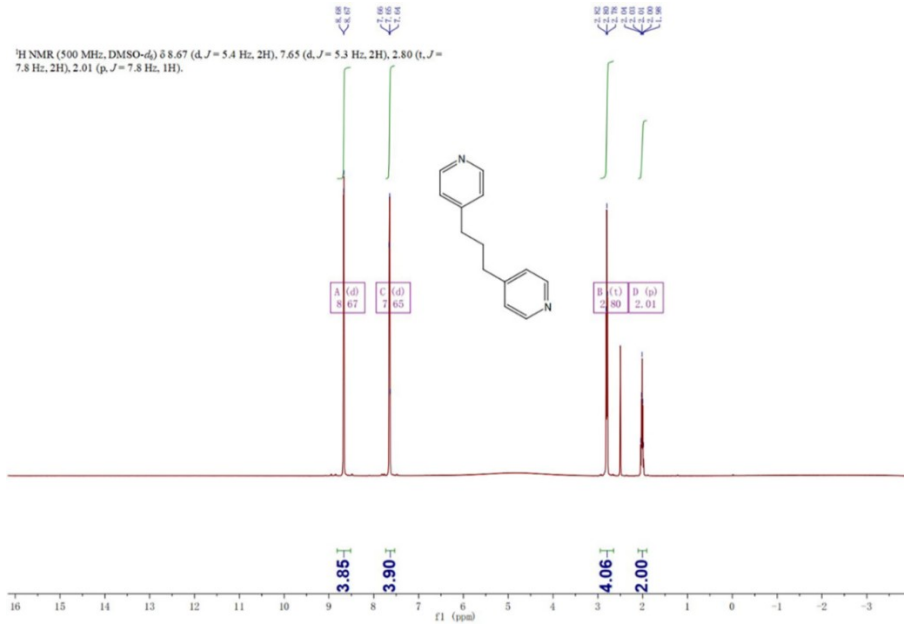

Fig. S13. ^{1}H-NMR of $TMDPSn_2Br_6$ measured in DMSO-d6.

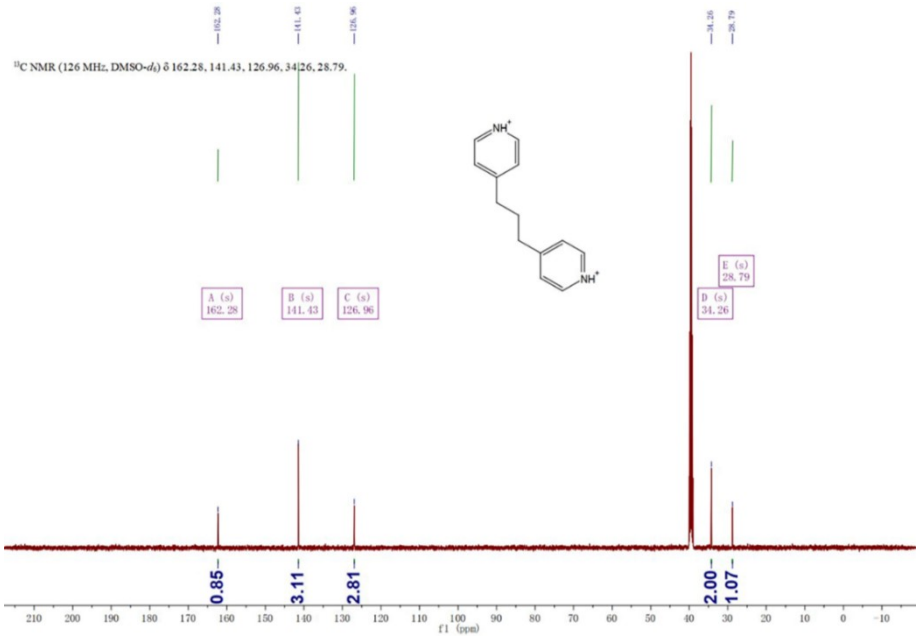

Fig. S14. ^{13}C-NMR of $TMDPSnBr_6$ measured in DMSO-d6.

Fig. S15. ^{1}H-NMR of $TMDPSnBr_6$ measured in DMSO-d6.

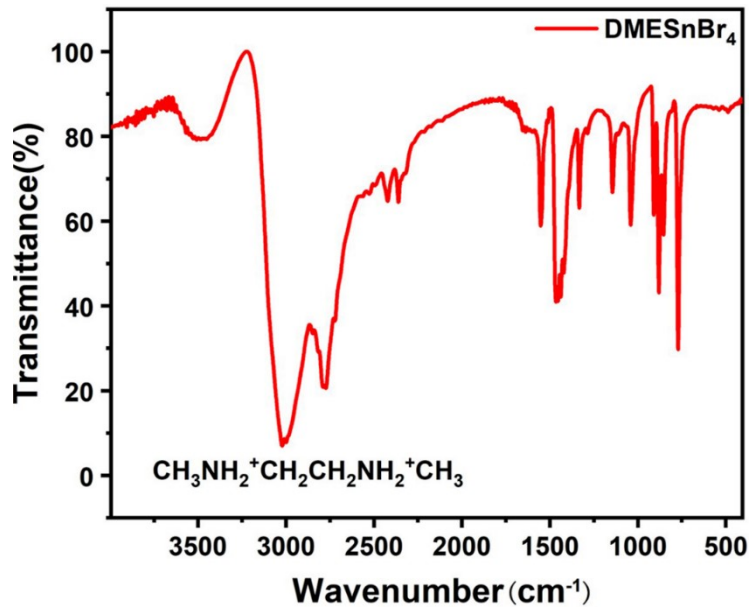

Fig. S16. FTIR spectrum of $DMESnBr_4$ measured by using KBr pellet method.

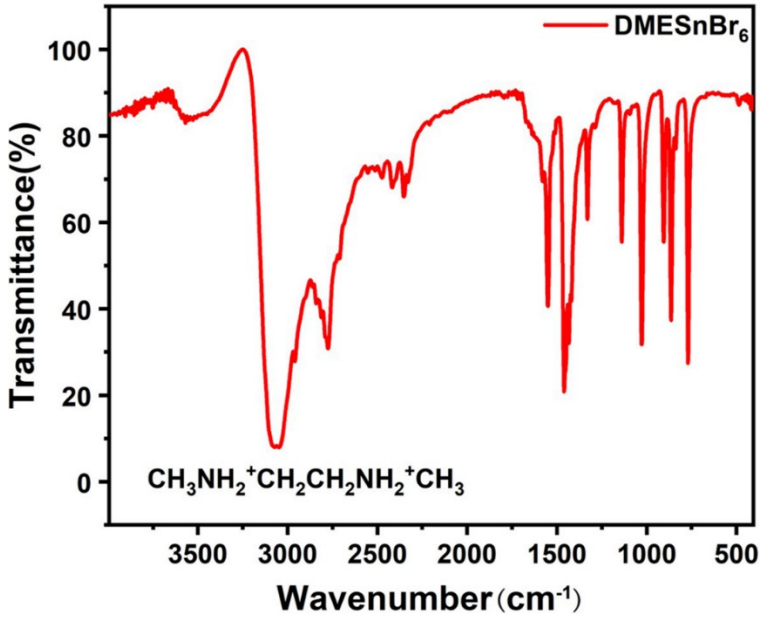

Fig. S17. FTIR spectrum of $DMESnBr_6$ measured by using KBr pellet method.

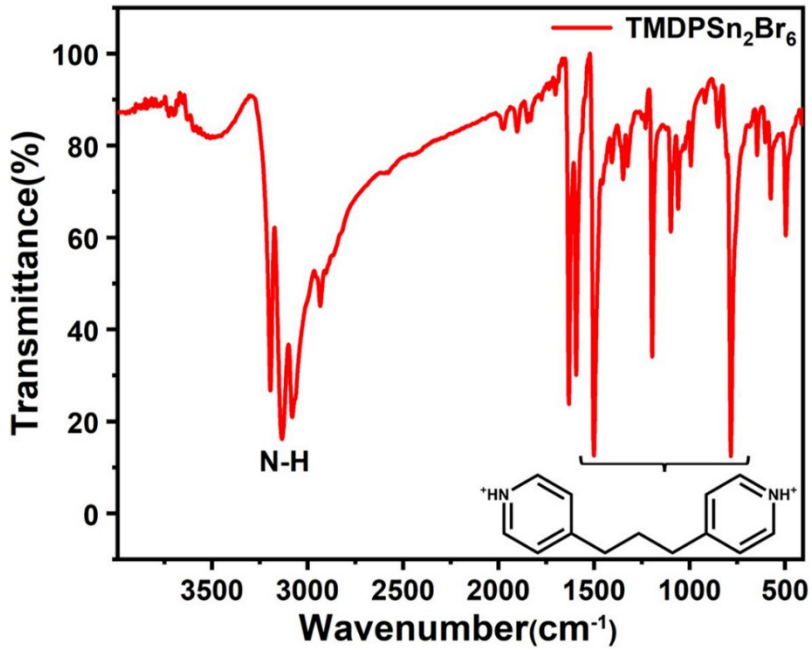

Fig. S18. FTIR spectrum of $TMDPSn_2Br_6$ measured by using KBr pellet method.

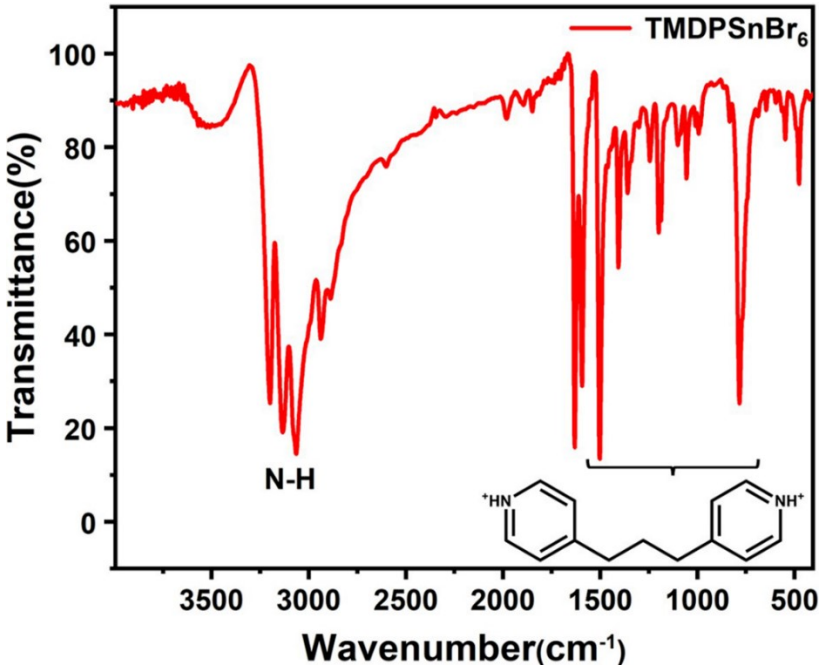

Fig. S19. FTIR spectrum of $TMDPSnBr_6$ measured by using KBr pellet method.

Table. IR Spectral Data (KBr pellet, cm^{-1}).

Compound	Peak position
$DMESnBr_4$	3021 cm^{-1}(vs), 3000 cm^{-1}(vs), 2959 cm^{-1}(s).
$DMESnBr_6$	3073 cm^{-1}(vs), 3047 cm^{-1}(vs), 2959 cm^{-1}(s).
$TMDPSn_2Br_6$	3064 cm^{-1}(vs), 1502 cm^{-1}(vs), 783 cm^{-1}(s).
$TMDPSnBr_6$	3134 cm^{-1}(vs), 1500 cm^{-1}(vs), 783 cm^{-1}(s).

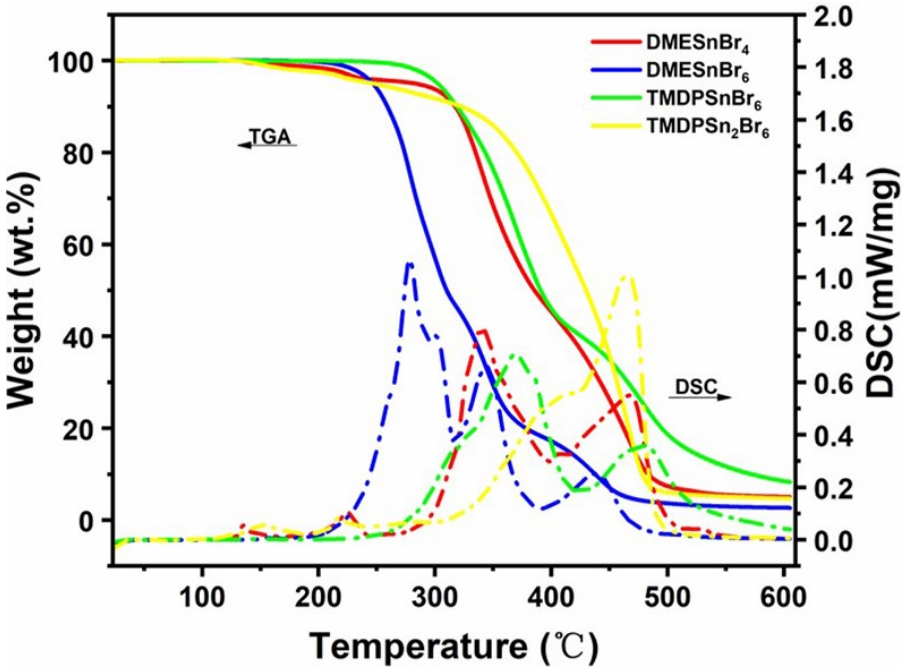

Fig. S20. TGA/DSC of $DMESnBr_m$ (m=4 or 6) and $TMDPSn_nBr_6$ (n=1 or 2).

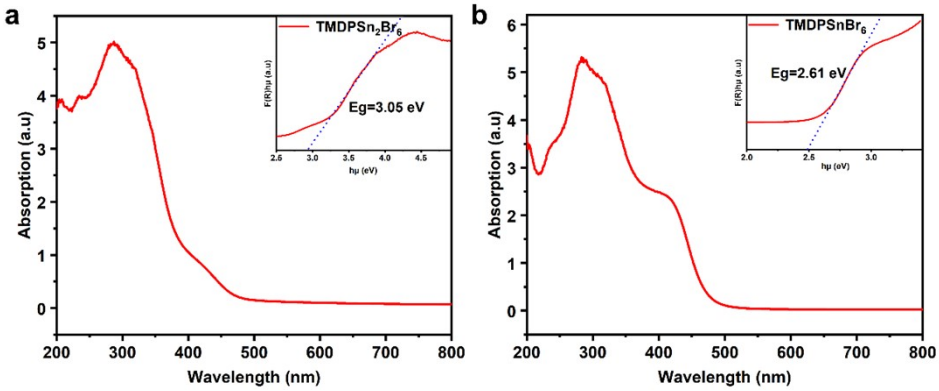

Fig. S21. Solid state UV-vis diffuse spectra at room temperature of a) $TMDPSn_2Br_6$ and b). $TMDPSnBr_6$. (The insets of a) and b) are tauc plots showing the calculated optical band gap).

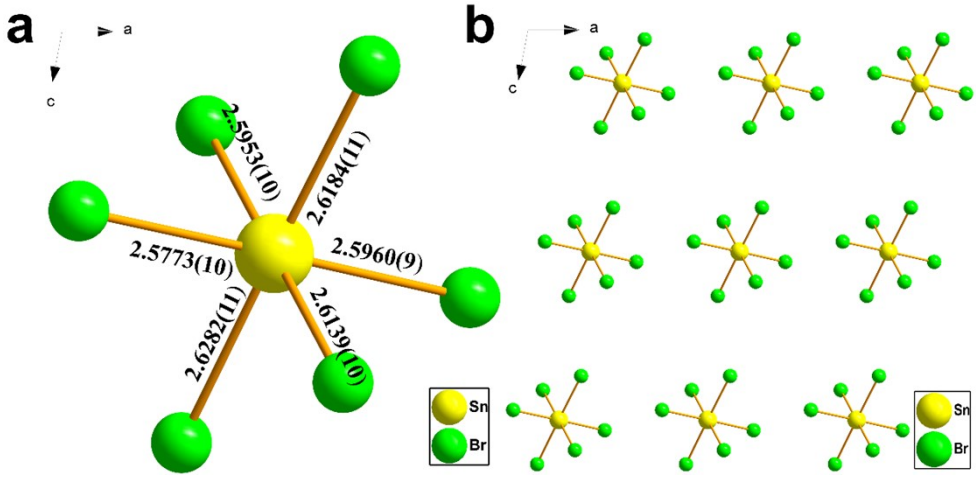

Fig. S22. {$SnBr_6$} units and ball-stick diagrams in the crystal structure of $DMESnBr_6$.

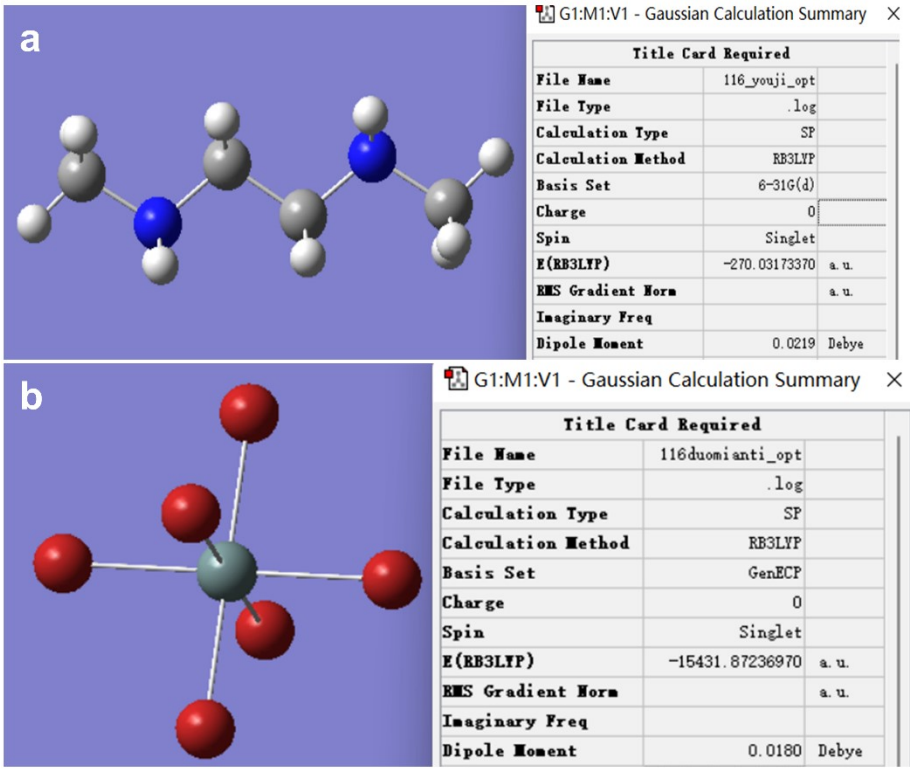

Fig. S23. The dipole moments of organic and inorganic parts in the crystal structure of $DMESnBr_6$ using Gaussian 09 program using B3LYP functional.

Table S1. Crystal data of $DMESnBr_4$、$DMESnBr_6$、$TMDPSn_2Br_6$ and $TMDPSnBr_6$.

Identification code	**$DMESnBr_4$**	**$DMESnBr_6$**	**$TMDPSn_2Br_6$**	**$TMDPSnBr_6$**
Empirical formula	$C_4H_{14}Br_4N_2Sn$	$C_4H_{14}Br_6N_2Sn$	$C_{13}H_{16}Br_6N_2Sn_2$	$C_{13}H_{16}Br_6N_2Sn$
Formula weight	528.50	688.32	917.12	798.43
Temperature/K	293.15	293.15	293(2)	293.15
Crystal system	Monoclinic	Monoclinic	Monoclinic	Monoclinic
Space group	*C*2/m（no.12）	$P2_1$（no.4）	*P*2/c（no.13）	$P2_1$/c（no.14）
a/Å	15.7498(16)	7.1983(6)	10.7946(3)	8.9183(10)
b/Å	14.5119(15)	13.5342(12)	4.63560(10)	21.856(2)
c/Å	6.1502(6)	8.2833(8)	22.9267(6)	11.2936(12)
α/°	90	90	90	90
β/°	111.880(3)	100.687(3)	101.1280(10)	106.313(4)
γ/°	90	90	90	90
Volume/$Å^3$	1304.4(2)	792.99(12)	1125.67(5)	2112.8(4)
Z	4	2	2	4
$\rho_{calc}g/cm^3$	2.691	2.883	2.706	2.510
μ/mm^{-1}	14.168	16.697	12.867	12.554
F(000)	968.0	624.0	836.0	1472.0
Crystal size/mm^3	0.15 × 0.12 × 0.1	0.1 × 0.08 × 0.05	0.15 × 0.12 × 0.08	0.18 × 0.15 × 0.1
Radiation	MoKα (λ = 0.71073)	MoKα (λ = 0.71073)	MoKα (λ = 0.71073)	MoKα (λ = 0.71073)
2Θ range for data	5.574 to 59.19	5.004 to	5.77 to 52.744	4.194 to 58.366

collection/°		59.196		
Index ranges	$-21 \le h \le 21$, $-20 \le k \le 20$, $-6 \le l \le 8$	$-9 \le h \le 9$, $-18 \le k \le 17$, $-11 \le l \le 11$	$-13 \le h \le 13$, $-5 \le k \le 5$, $-28 \le l \le 28$	$-12 \le h \le 12$, $-29 \le k \le 25$, $-15 \le l \le 15$
Reflections collected	10403	12815	9707	33977
Independent reflections	1898 [R_{int} = 0.0499, R_{sigma} = 0.0413]	4333 [R_{int} = 0.0374, R_{sigma} = 0.0504]	2300 [R_{int} = 0.0410, R_{sigma} = 0.0377]	5690 [R_{int} = 0.0680, R_{sigma} = 0.0540]
Data/restraints/parameters	1898/0/57	4333/1/121	2300/0/106	5690/0/200
Goodness-of-fit on F^2	1.030	1.020	1.057	1.026
Final R indexes [I>=2σ (I)]	R_1 = 0.0373, wR_2 = 0.0869	R_1 = 0.0285, wR_2 = 0.0526	R_1 = 0.0323, wR_2 = 0.0908	R_1 = 0.0365, wR_2 = 0.0677
Final R indexes [all data]	R_1 = 0.0636, wR_2 = 0.0970	R_1 = 0.0405, wR_2 = 0.0551	R_1 = 0.0398, wR_2 = 0.0951	R_1 = 0.0789, wR_2 = 0.0786
Largest diff. peak/hole / e $Å^{-3}$	2.33/-0.70	0.60/-0.66	0.92/-0.70	1.00/-0.88
Flack parameter	-	0.041(9)	-	-

Table S2. Selected bond lengths (Å) and Bond Valences for $DMESnBr_4$、$DMESnBr_6$、$TMDPSn_2Br_6$ and $TMDPSnBr_6$.

	Atom	Bond length R_{ij} (Å)	R_0	B	Bond Valence S_{ij}
$DMESnBr_4$	Sn1				1.65
	Br1	2.9978	2.53	0.35	-0.26
	Br2	2.9978	2.53	0.35	-0.26
	Br3	2.7195	2.53	0.35	-0.58
	Br4	2.742	2.53	0.35	-0.55
$DMESnBr_6$	Sn1				3.50
	Br1	2.5772	2.4	0.37	-0.62
	Br2	2.596	2.4	0.37	-0.63
	Br3	2.6137	2.4	0.37	-0.56
	Br4	2.5953	2.4	0.37	-0.59
	Br5	2.6282	2.4	0.37	-0.54
	Br6	2.6183	2.4	0.37	-0.55
$TMDPSn_2Br_6$	Sn1				1.70
	Br1	2.7619	2.53	0.35	-0.52
	Br2	2.6969	2.53	0.35	-0.62
	Br3	2.7307	2.53	0.35	-0.56
$TMDPSnBr_6$	Sn1				3.51
	Br1	2.6263	2.4	0.37	-0.54
	Br2	2.6353	2.4	0.37	-0.53
	Br3	2.5701	2.4	0.37	-0.63
	Br4	2.6205	2.4	0.37	-0.55
	Br5	2.5732	2.4	0.37	-0.63
	Br6	2.5739	2.4	0.37	-0.63

References:

1. O. V. Dolomanov, L. J. Bourhis, R. J. Gildea, J. A. K. Howard and H. Puschmann, OLEX2: a complete structure solution, refinement and analysis program, *J. Appl. Crystallogr.*, 2009, **42**, 339-341.
2. L. J. Bourhis, O. V. Dolomanov, R. J. Gildea, J. A. Howard and H. Puschmann, The anatomy of a comprehensive constrained, restrained refinement program for the modern computing environment - Olex2 dissected, *Acta Crystallogr. A Found Adv.*, 2015, **71**, 59-75.
3. G. M. Sheldrick, A short history of SHELX, *Acta Crystallogr. A*, 2008, **64**, 112-122.
4. W. Song, K. Leung, Q. Shao, K. J. Gaskell and J. E. Reutt-Robey, Complexation and Phase Evolution at Dimethylformamide–Ag(111) Interfaces, *J. Phys. Chem. C*, 2016, **120**, 22979-22988.
5. S. K. Kurtz and T. T. Perry, A Powder Technique for the Evaluation of Nonlinear Optical Materials, *J. Appl. Phys.*, 1968, **39**, 3798-3813.
6. G. Kresse and J. Furthmüller, Efficiency of ab-initio total energy calculations for metals and semiconductors using a plane-wave basis set, *Comp. Mater. Sci.*, 1996, **6**, 15-50.
7. G. Kresse and J. Furthmuller, Efficient iterative schemes for ab initio total-energy calculations using a plane-wave basis set, *Phys. Rev. B Condens. Matter*, 1996, **54**, 11169-11186.
8. J. P. Perdew, K. Burke and M. Ernzerhof, Generalized Gradient Approximation Made Simple, *Phys. Rev. Lett.*, 1996, **77**, 3865-3868.
9. J. P. Perdew, K. Burke and M. Ernzerhof, Generalized Gradient Approximation Made Simple [Phys. Rev. Lett. 77, 3865 (1996)], *Phys. Rev. Lett.*, 1997, **78**, 1396-1396.
10. H. J. Monkhorst and J. D. Pack, Special points for Brillouin-zone integrations, *Phys. Rev. B*, 1976, **13**, 5188-5192.